Matching Vector Filtering Methods For Sea Ice Motion Detection Using SAR Imagery Feature Tracking

Chaoyue Li, Gang Li, Zhuoqi Chen, Xue Wang, and Xiao Cheng

***Abstract*—Applying feature tracking techniques to synthetic aperture radar (SAR) imagery generates high-resolution sea ice motion fields. However, the bad matching vectors still exist after the Nearest Neighbor Distance Ratio test and contaminate the derived motion fields, which need to be identified and filtered out. In this article, we propose two algorithms to eliminate such wrong matching vectors. The first employs the matching results derived by the maximum cross-correlation (MCC) method as the reference motion fields to evaluate such wrong matches. The second method employs the local spatial consistency presumption of sea ice motion fields. A Voronoi diagram is applied to slice the overlapping area of two SAR images into many fractions, and each fraction extends its size 50% outward to calculate the regional mean sea ice flow vector and standard deviation. Any vector within the fraction that exceeds 3 times the regional standard deviation will be recognized as an outlier and filtered out. Two methods are tested to two cases with strong rotation or irregular sea ice motion fields derived from Sentinel-1 imagery. The overall accuracy of our two methods is 93.9% and 98.7%, and they sacrifice 6.12% /1.22% of the correct vectors to filter out 100.0% / 94.12% of the wrong vectors for the MCC referenced filter and Voronoi fragmented filter, respectively.**

***Index Terms*—Feature tracking, image matching, sea ice motion, synthetic aperture radar (SAR).**

I. Introduction

SEA ice is an essential part of the Arctic cryosphere, which is of great significance to the study of global climate change and Arctic shipping [1]. Sea ice is driven by the force of the weather system and ocean current, and has a direct impact on regional hydrology and climate [2]. With the rapid development of satellite remote sensing technology, a large number of satellite observation data are applied to sea ice motion monitoring. Microwave radiometers and microwave scatterometers are widely used in sea ice motion monitoring because of their wide spatial coverage and daily revisiting, but their spatial resolutions are usually low, most of them are coarser than 10 km [3], [4]. Similar to the scatterometer, synthetic aperture radar (SAR) is not affected by cloud or polar night, can also be applied to monitor sea ice motion but to derive finer resolution motion fields than radiometer and scatterometer [5].

There are two kinds of algorithms for sea ice motion monitoring based on SAR imagery. The first is based on template matching method including maximum cross-correlation (MCC), normalized cross-correlation [6], and phase correlation [7]. Template matching slices a reference window of one acquisition on a searching window of another acquisition, regarding the location of best matching as the offset of two acquisitions [8]. Such coregistration can also be calculated in the frequency domain [7]. Another method is feature tracking, which detects the feature points on the primary and secondary imagery. The feature points of two imageries are matched after being described by high-dimensional descriptors, then the sea ice motion vectors are calculated based on the offset value of matched points. Different feature point operators generate different results of sea ice motion field in terms of accuracy and vector density [9]. It finds that accelerated KAZE (A-KAZE) performs best on sea ice motion deriving than other features in terms of both calculation efficiency and coverage by testing scale invariant feature transform, oriented features from accelerated segment test (FAST) and rotated brief, and A-KAZE to Sentinel-1 imagery [10].

In the feature tracking processes, the best candidate matched from the secondary image for each feature point from the primary image is found by identifying its nearest neighbor feature point, which is defined as the feature with the minimum Hamming distance [11]. Usually, brute force or fast library for approximate nearest neighbors (FLANN) matchers are used for matching. Inevitably, speckle and thermal noise on SAR images generate wrong matches [12], then yield bad sea ice motion vectors. There are usually two methods to solve such problem: the random sample consensus (RANSAC) algorithm and the Nearest Neighbor Distance Ratio (NNDR) algorithm. RANSAC algorithm can effectively filter out the wrong matches from a large number of matches by calculating the homography function between matching points, usually applied in object tracking [13]. NNDR test compares the distance of the nearest neighbor to the second-closest neighbor. This method works

Manuscript received 10 March 2022; revised 7 June 2022 and 30 June 2022; accepted 31 July 2022. Date of publication 3 August 2022; date of current version 10 August 2022. This work was supported in part by the National Key Research and Development Program of China under Grant 2019YFC1509104, in part by the National Natural Science Foundation of China under Grant 41901384, in part by Science and Technology Projects in Guangzhou under Grant 20210202033, and in part by the Innovation Group Project of Southern Marine Science and Engineering Guangdong Laboratory (Zhuhai) under Grant 311021008. *(Corresponding author: Gang Li.)*

The authors are with the School of Geospatial Engineering and Science, Sun Yat-sen University, Guangzhou 510275, China, and also with the Southern Marine Science and Engineering Guangdong Laboratory, Zhuhai 519082, China (e-mail: lichy88@mail2.sysu.edu.cn; ligang57@mail.sysu.edu.cn; chenzhq67@mail.sysu.edu.cn; wangxue25@mail.sysu.edu.cn; chengxiao9@mail.sysu.edu.cn).

Digital Object Identifier 10.1109/JSTARS.2022.3196026

TABLE I
DETAIL INFORMATION OF SAR IMAGES

IMAGE GROUP	TIME	SATELLITE	PATH	FRAME	FLIGHT DIRECTION
1	11/22/19, 05:46:25	SENTINEL-1B	110	283	ASCENDING
	11/24/19, 05:30:02	SENTINEL-1B	139	284	ASCENDING
2	04/14/20, 10:43:26	SENTINEL-1B	113	293	DESCENDING
	04/16/20, 08:48:49	SENTINEL-1B	141	300	DESCENDING

well because the good matched feature points have the closest correct neighbor feature points, which should be significantly closer than the second closest feature point. When the distance ratio of the second closest match and the closest match is greater than 0.8, the match is recognized as a wrong match, this method eliminates 90% of wrong matches while discarding less than 10% of the correct matches [12].

After the NNDR test, a postprocessing algorithm is necessary to filter out the remaining wrong matches. Demchev et al. [10] proposed that bad sea ice motion vectors could be checked by considering the discrepancy with other adjacent vectors within a certain distance. Aiming at identifying and removing the bad matches after performing the NNDR algorithm with high accuracy and efficiency, this study proposes and compares two novel postprocessing methods.

II. DATA DESCRIPTION

C-band Sentinel-1 A/B SAR constellation operates in a near-polar and solar synchronous orbit with a repetition period of 12 days and 6 days for single or dual satellites, respectively. Since the orbital spacing narrows with the increase of latitude, the revisiting cycle in the Arctic is much less than 6 days, offering an opportunity to perform rapid sea ice motion monitoring. The extra wide (EW) mode images adopt by this research have a moderate spatial resolution (40 $\times$ 40 m, medium resolution product) and large swath width (410 km), including HH and HV polarization channels.

Two pairs of Sentinel-1 images observed in the Arctic ocean obtained in November 2019 and April 2020 are tested, and the acquisition interval for each pair is about 2 days. Table I tabulates the detailed information of these images, and Fig. 1 presents their spatial coverage.

API module "snappy" provided by the sentinel application platform (SNAP) in Python is applied for image preprocessing, including importing precise orbit and calibration. We used ellipsoid correction to reproject SAR images into the polar stereographic (EPSG:3413) grid with 100 $\times$ 100 m resolution.

III. METHODOLOGY

A. Sea Ice Vector Extraction Based on Feature Tracking

The main working flow of sea ice motion vector extraction based on feature tracking is described as follows. The first step is to preprocess two SAR images and generate A-KAZE feature points, then use the brute force matcher to match the feature points. Second, we calculate the motion speed and motion direction of matching points to get all matching drift vectors. The third step is to filter out the wrong matching vectors. The working flow is shown in Fig. 2.

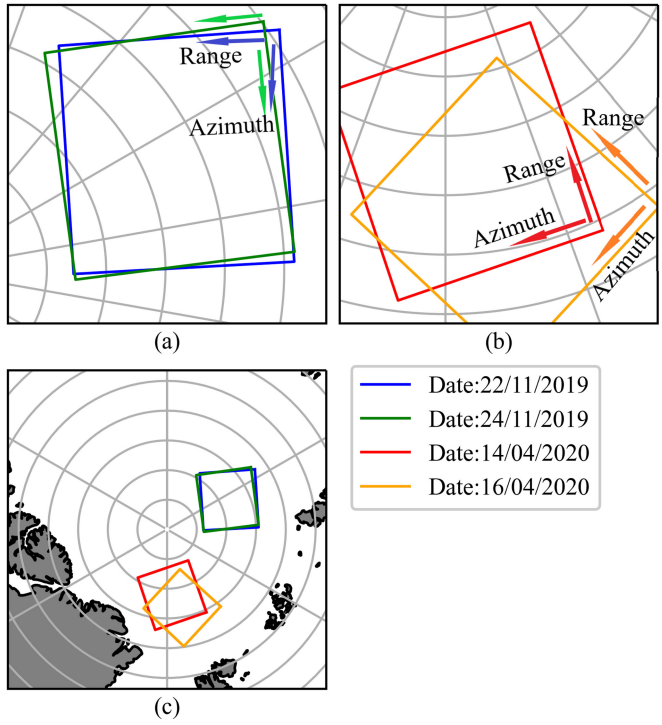

Fig. 1. Spatial location information of images.

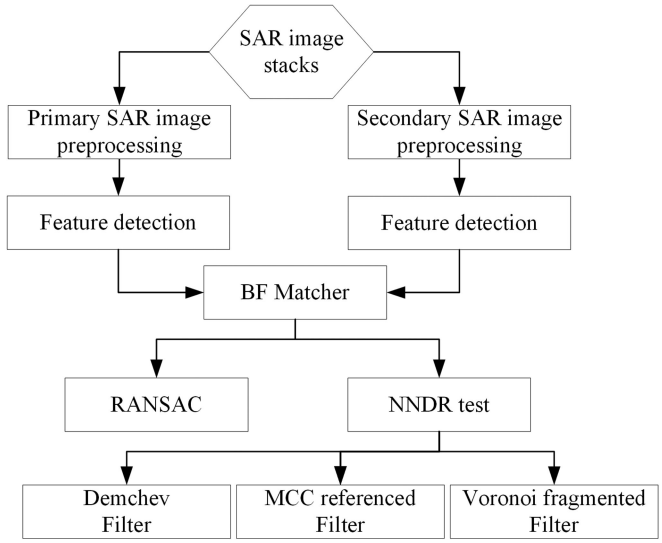

Fig. 2. Working flow of vector extraction method.

Before filtering wrong drift vectors, we filter out vectors starting or ending on land using a coastal mask. RANSAC and NNDR algorithms are two optional methods to remove wrong drift vectors. The threshold of RANSARC reprojection is set as 8.0. For the NNDR algorithm, the distance ratio between the second-best match to the best match is set to 0.8, which could filter out 90% wrong vectors at the cost of 10% correct vectors [12]. After the NNDR algorithm, we test the two post-processing algorithms proposed in this study for further filtering,

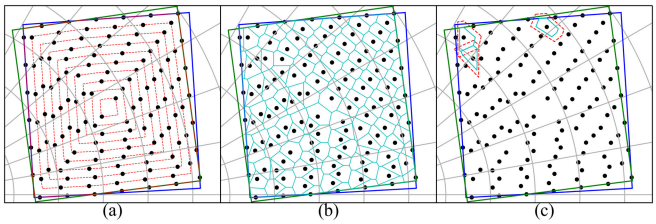

Fig. 3. Schematic of filtering algorithm based on Voronoi diagram.

and compare them with the RANSAC algorithm and Demchev's algorithm [10].

B. Demchev's Filter

Demchev et al.'s [10] filtering algorithm requires that all drift vectors are checked by its correlation with the vectors in the adjacent region. Drift vectors, which meet the following criteria, can be considered as the correct vectors.

1) There are at least eight neighboring drift vectors.
2) The length of the vector does not exceed 1σ of the weighted median vector.
3) The vector's direction is consistent with its four neighborhoods.

C. MCC Referenced Filter

The MCC matching method is employed to generate a reference sea ice motion field. The spatial resolution of the Sentinel-1 EW image is processed as 320 × 320 m through 8 × 8 multilook. The template size is 9 × 9 and the step size is 5 × 5. Matchings with correlation coefficient above 0.92 is taken as correct matches. For each sea ice drift vector obtained by feature tracking, the nearest template matching vector derived with MCC is taken as the reference. When the velocity difference between feature tracking derived by feature tracking and the MCC reference vector is greater than 0.1m/s (∼8.6km/d) or the difference of flow directions is greater than 10°, the feature-tracking-derived vector is recognized as a wrong vector and be eliminated.

D. Voronoi Fragmented Filter

Sea ice motion should be homogenous in a small area [14]; here, we propose another method to filter the wrong vector. The first step is to scale the boundary lines of the overlapping area of two SAR images and take points at an equal distance on all boundaries, as shown in Fig. 3(a). We determine the number of points each time according to the following:

$$n_{(x)} = \frac{n_1}{f} \cdot (f + 1 - x) \tag{1}$$

where $n_{(x)}$ represents the number of points taken on a layer (outermost layer $x = 1$), and f represents the total number of layers. Second, all the points are used as discrete points to construct the Voronoi diagram, as shown in Fig. 3(b). By this method, multiple polygons with similar size and shape within the overlap of two images are formed. Third, each polygon expands outward by 50% [see red dash polygon in Fig. 3(c)] by distance

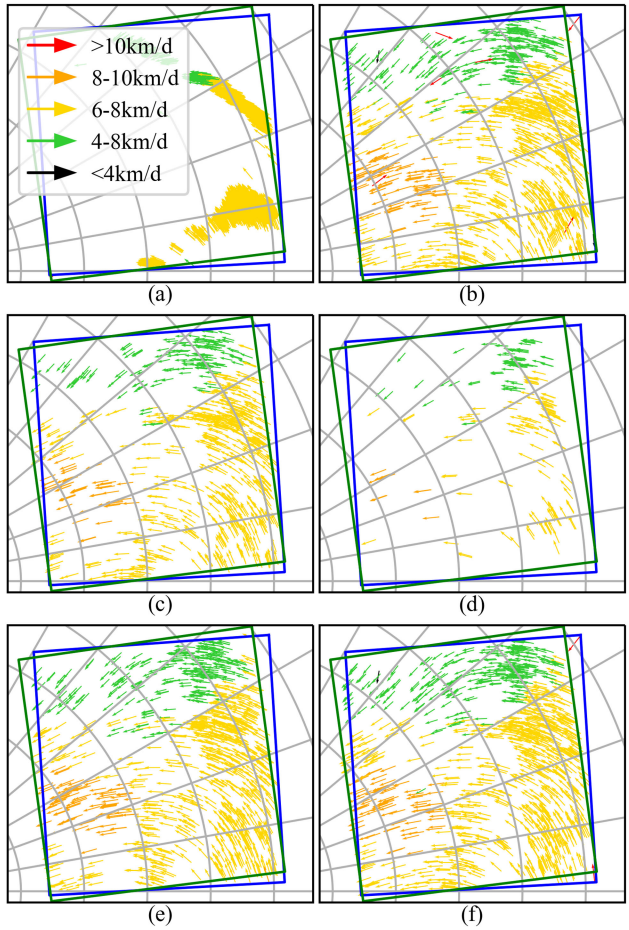

Fig. 4. Results of matching of different filters for image pair 1. (a) RANSAC. (b) NNDR. (c) Demchev's filter. (d) MCC vectors. (e) MCC referenced filter. (f) Voronoi fragmented filter.

to evaluate the regional average speed and direction of sea ice motion and their standard deviations. The average speed and its standard deviation are calculated by taking the drift vector as scale. The average direction is calculated by the vector sum of all flow vectors within the dash red polygon. Direction deviations are calculated by applying the law of cosines to the average vector and each vector. Each vector inside the unexpanded polygon [see cyan polygon in Fig. 3(b) and (c)] is then checked. For each vector, when the speed or flow direction difference between the vector and its regional average exceeds 3 times of the regional standard deviation, the vector is considered as a bad match and be eliminated.

IV. Experimental Results and Discussion

A. Sea Ice Motion Fields

The results of different vector filtering methods are shown in Figs. 4 and 5, corresponding to image pairs 1 and 2, respectively. Figs. 4(a) and 5(a) show the results of the RANSAC algorithm. Although the wrong vectors are filtered, a considerable number of correct vectors are also removed, resulting in large vacancies in the overlap areas. Figs. 4(b) and 5(b) show the results filtered resulted by the NNDR algorithm, obviously several error vectors survived. Figs. 4(c) and 5(c) show the results filtered resulted by

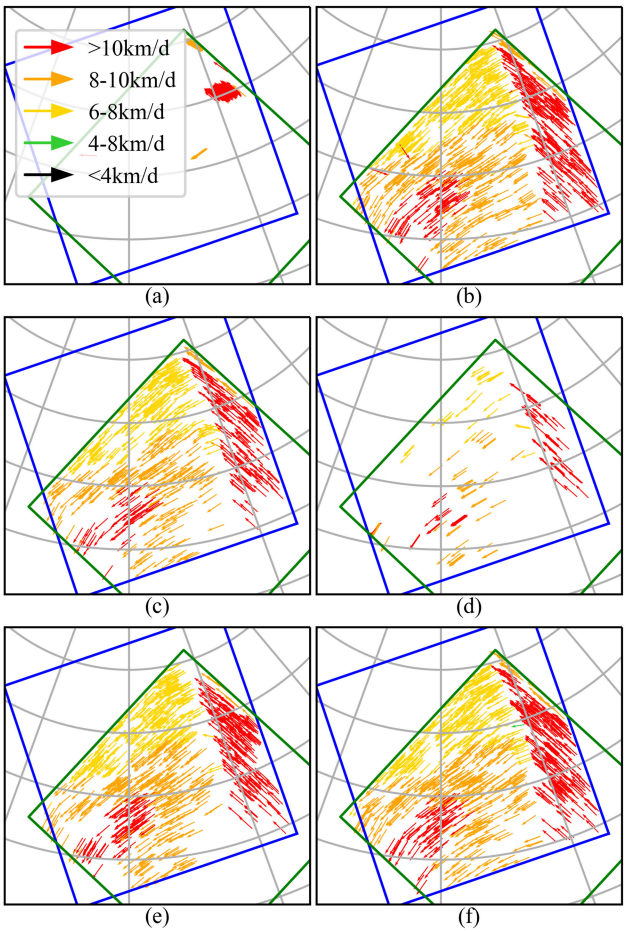

Fig. 5. Results of matching of different filters for image pair 2. (a) RANSAC. (b) NNDR. (c) Demchev's filter. (d) MCC vectors. (e) MCC referenced filter. (f) Voronoi fragmented filter.

TABLE II
RESULTS OF DIFFERENT FILTER METHOD

PAIRS	FILTER METHOD	DEAL TIME(S)	VECTOR NUMBER	COVERING RATIO
1	RANSAC	2.08	2344	8.56%
	NNDR	0.07	11254	75.29%
	DEMCHEV	77.20	7676	55.49%
	MCC	1394.82	10675	70.29%
	VORONOI	17.93	11044	73.69%
2	RANSAC	1.29	183	1.37%
	NNDR	0.05	10378	83.85%
	DEMCHEV	65.99	7186	70.40%
	MCC	1031.18	9538	76.20%
	VORONOI	15.69	10216	81.92%

Demchev's filter. Figs. 4(d) and 5(d) show reference sea ice motion fields derived by the MCC method. Figs. 4(e) and 5(e) show the survived vectors after MCC referenced filter. Figs. 4(f) and 5(f) show the filtered results based on Voronoi fragmentation filter. Considering the visual effect, the vector data in the figures are diluted to 1/10 for all subplots except (a) and (d).

Table II tabulates the results of each method, in which deal time only records the filtering step (including forming MCC referenced motion fields); RANSAC algorithm shows high efficiency, whereas the MCC referenced filter has the lowest efficiency, as it consumed a long time in template matching, with 1015 and 802 s in two pairs, respectively, accounting for 72%–77% of the total running time (see Table II). All vectors need to be checked with all template matching results to query the nearest reference vector before checking difference of speed and angle. For Demchev's filter, all vectors must be compared with all other vectors to obtain the number and distance of surrounding vectors, which consumes long time. If the total number of drift vectors increases, the efficiency of this filtering algorithm will be further reduced. The Voronoi fragment filter only needs to traverse all vectors once to confirm which Voronoi diagram they belong to, and generating Voronoi polygons dominates its running time, which means even if the number of drift vectors increases, the overall time consumption of this filter will not increase significantly.

The vector number is the count of survived sea ice drift vectors after filtering, and the coverage ratio represents the ratio of the vectors covering area with the total overlap area of two SAR images. To calculate covering area, each vector is dilated to a circle with radius of 5 km from its star point, and then, calculate the total covered area. Overlapped area of circles is counted only once.

Three postprocess filters preserve enough matching vectors to show similar covering ratios as the results given by NNDR test, while most of the wrong bad matches are filtered out. Three filters preserve significantly more area than RANSAC algorithms. The number of vectors saved by Demchev's filter about 30% less than two proposed filters. Although the vectors preserved by Demchev's filter can cover the most of the overlap area, the coverage ratio is lower, which means less details of the derived sea ice motion fields. Two filters proposed in this article saved more correct vectors and larger coverage ratios by only sacrificing a few vectors or a small covering area, especially for image pair 2, where sharp changes of the sea ice motion fields are found.

Fig. 6 selected two zones each of the image pairs 1 and 2 to present the detail results of different filtering methods. Each selected area covers about 25 km^2. Subplots in Fig. 6(a), (e), (i), and (m) show the results after NNDR test. Wrong matches are manually identified and marked with black circles. Subplots in Fig. 6(b), (f), (j), and (n) show the drift vector filtered by Demchev's filter. Subplots in Fig. 6(c), (g), (k), and (o) show MCC referenced filter. Subplots in Fig. 6(d), (h), (l), and (p) show the drift vectors filtered by Voronoi fragmented method. All three methods effectively filter out the wrong vectors.

B. Accuracy Analysis

The total number of all vectors after NNDR test in pair 1 is 11 254, including 11 177 correct vectors and 77 wrong vectors. The total number of all vectors after NNDR test in pair 2 is 10 378, including 10 340 correct vectors and 38 wrong vectors. Tables III and IV tabulate the detailed classification accuracy of two proposed method and Demchev's.

Table III compares of the ability of retaining vectors for different methods. For image pair 1, Demchev's filter saved 7676 correct vectors, accounting for 7676/11 177 = 68.68% of all correct vectors. MCC referenced filter retains 10 675 correct vectors, accounting for 10 675/11 177 = 95.51% of all correct

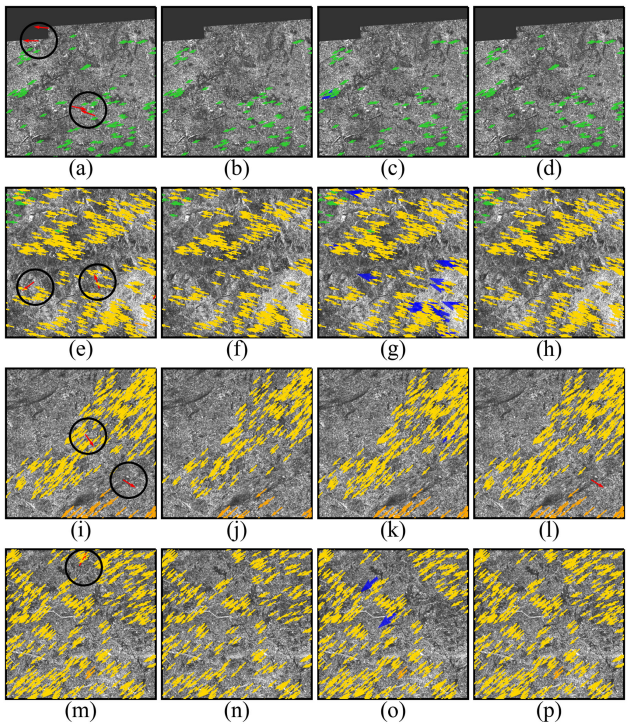

Fig. 6. Results of different filters in several selected areas of image pairs 1 and 2. (a)–(h) are the area of image pair 1 and (i)–(p) are the area of images pair 2. (a), (e), (i), and (m) are the results after NNDR test. (b), (f), (j), and (n) are the results of Demchev's filter. (c), (g), (k), and (o) are the results of MCC referenced filter. MCC vector is displayed in blue and bold. (d), (h), (l), and (p) shows the results of Voronoi fragmented filter.

TABLE III
NUMBERS OF SURVIVED VECTORS

PAIRS	FILTER METHOD	SURVIVED VECTORS	CORRECT VECTORS	BAD VECTORS	SURVIVED RATE
1	DEMCHEV	7676	7676	0	68.68%
	MCC	10675	10675	0	95.51%
	VORONOI	11044	11039	5	98.77%
2	DEMCHEV	7186	7186	0	69.50%
	MCC	9538	9538	0	92.24%
	VORONOI	10216	10214	2	98.78%

TABLE IV
NUMBERS OF FILTERED VECTORS

PAIRS	FILTER METHOD	FILTERED VECTORS	CORRECT VECTORS	BAD VECTORS	FILTERED RATE
1	DEMCHEV	3578	3501	77	100.00%
	MCC	579	502	77	100.00%
	VORONOI	210	138	72	93.51%
2	DEMCHEV	3192	3154	38	100.00%
	MCC	840	802	38	100.00%
	VORONOI	162	126	36	94.74%

vectors, without any wrong vectors. The Voronoi fragment filter retains 11 174 correct vectors, accounting for 11 039/11 177 = 98.76% of the total correct vectors, and 20 wrong vectors. All three filters will filter out correct vectors. The results in pair 2 are similar.

Table IV tabulates the detailed information of filtered vectors. Both Demchev's filter and MCC referenced filter in mage pair 1 filters out all of wrong vectors. But they also filter out 3501/11 177 = 31.32% and 502/11177 = 4.49% of all the correct vectors. The wrong vectors filtered by Voronoi fragment filter are less, accounting for 72/77 = 93.51% of all error vectors, but only 138/11 177 = 1.23% of the correct vectors are filtered. The results are similar in image pair 2.

The overall accuracies of Demchev's filter for two image pairs are (7676 + 77)/11 254 = 68.89% and (7186 + 38)/10 378 = 69.61%, respectively. For MCC referenced filter, the overall accuracies are (10 675 + 77)/ 11 254 = 95.54% and (9538 + 38)/ 10 378 = 92.27%. For Voronoi fragment filter, the overall accuracies is (11 039 + 72)/11 254 = 98.73% and (10 214 + 36)/10 378 = 98.77%.

It finds that MCC referenced filter has stronger ability to filter error vectors than Voronoi fragmented filter, but the latter can retain more correct vectors. MCC referenced method compares feature-tracking-derived vector to its nearest MCC-derived vector, and discard the former if speed or flow direction difference exceed the threshold. This means a bad MCC-derived vector can contaminate all its feature tracking neighbor vectors. Such strategy may also wrongly kill the correct vectors if spatial distance between feature-tracking-derived vector is too far to its nearest MCC-derived vector, as MCC-derived vectors [see Figs. 4(d) and 5(d)] are obviously much sparser than the A-KAZE-derived vectors [see Fig. 4(d) and (b)].

For Voronoi fragmented filter, most survived wrong vectors locate in the edge of the overlapped area of two SAR images, where area of each polygon are smaller than other polygons, resulting the average speed and direction may not be as accurate as other polygons. Another possible reason is vectors are supposed to be sparse at the edge of the overlapping area because feature vectors may flow in or out of this area and cannot be matched from two images.

Our comparison finds that Demchev's filter tends to wrongly remove correct vectors, especially at the border of the overlap area. This could be due to not enough neighboring drift vectors can be found, similar as our proposed Voronoi fragmented filter. Our proposed method has a less strict setting, which could be the reason why it retains more correct matchings. Besides, the Voronoi fragmented only needs to assign each matching vector to its polygon, and Demchev's filter should traverse all vectors for each vector to find its several closest neighbors. This leads to the differences of calculation efficiency.

Since feature tracking with A-KAZE descriptor to Sentinel-1 SAR images usually generates vectors dense enough to describe sea ice motion fields, it recommends combining two proposed methods to ensure the accuracy of the derived motion fields if calculation efficiency is not a consideration and MCC reference fields are dense enough. MCC referenced filter requires extracting template matching vectors from the original SAR images. However, the original geocoded SAR image is not always available, such as usually the released sea ice motion fields only contain motion vectors, then our proposed Voronoi fragmented filter still works. Two images that selected in this research are extreme cases that with strong rotation or irregular sea ice motion fields, while most cases are not as extreme as these two pairs. Empirically, two filters proposed in this research also works well on the usual cases.

V. Conclusion

In this research, two algorithms are proposed to filter the wrong matching vectors for deriving sea ice motion field based on feature tracking to SAR imagery. The first employs the matching results derived by the MCC method as the reference motion fields to find wrong matches. The second method employs the Voronoi diagram to slice the overlapping area into many fractions. By regarding the local consistency of sea ice motion, any vector within the fraction that exceeds 3 times of the regional standard deviation will be recognized as an outlier and be filtered out. Testing on two extreme cases with strong rotation or irregular sea ice motion fields, and accuracy analysis based on manually identifying bad matches, it finds two proposed methods that can both effectively identify bad matches and preserve most correct matches for describing the sea ice motion fields. Overall accuracy of the Voronoi fragmented method is slightly higher than MCC referenced method but the latter filters out more bad matches, also consumes longer processing time. Sea ice motion fields derived by both of our proposed methods cover a larger area than Demchev's method, which could be due to their very strict criteria.

References

[1] J. C. Stroeve et al., "The arctic's rapidly shrinking sea ice cover: A research synthesis," *Climatic Change*, vol. 110, pp. 1005–1027, Feb. 2012, doi: 10.1007/s10584-011-0101-1.

[2] P. R. Holland and R. Kwok, "Wind-driven trends in antarctic sea-ice drift," *Nat. Geosci.*, vol. 5, pp. 872–875, Dec. 2012, doi: 10.1038/Ngeo1627.

[3] P. Heil et al., "A comparison of east antarctic sea-ice motion derived using drifting buoys and remote sensing," *Ann. Glaciol.*, vol. 33, pp. 139–144, 2001, doi: 10.3189/172756401781818374.

[4] M. Tschudi, W. N. Meier, J. S. Stewart, C. Fowler, and J. Maslanik, "Polar Pathfinder Daily 25 km EASE-Grid Sea Ice Motion Vectors, Version 4," NASA National Snow and Ice Data Center Distributed Active Archive Center, 2019. [Online]. Available: https://doi.org/10.5067/INAWUWO7QH7B

[5] S. Muckenhuber et al., "Open-source feature-tracking algorithm for sea ice drift retrieval from sentinel-1 SAR imagery," *Cryosphere*, vol. 10, pp. 913–925, 2016, doi: 10.5194/tc-10-913-2016.

[6] M. Thomas et al., "High resolution (400 m) motion characterization of sea ice using ERS-1 SAR imagery," *Cold Regions Sci. Technol.*, vol. 52, pp. 207–223, Apr. 2008, doi: 10.1016/j.coldregions.2007.06.006.

[7] M. Thomas, C. Kambhamettu, and C. A. Geiger, "Motion tracking of discontinuous sea ice," *IEEE Trans. Geosci. Remote Sens.*, vol. 49, no. 12, pp. 5064–5079, Dec. 2011, doi: 10.1109/Tgrs.2011.2158005.

[8] R. F. Wang et al., "Combined pattern matching and feature tracking for bohai sea ice drift detection using gaofen-4 imagery," *Int. J. Remote Sens.*, vol. 41, pp. 7486–7508, Oct. 2020.

[9] A. Satnik et al., "A comparison of Key-point descriptors for the stereo matching algorithm," in *Proc. 26th Int. Conf. Radioelektronika*, 2016, pp. 292–295.

[10] D. Demchev, V. Volkov, E. Kazakov, P. F. Alcantarilla, S. Sandven, and V. Khmeleva, "Sea ice drift tracking from sequential SAR images using Accelerated-KAZE features," *IEEE Trans. Geosci. Remote Sens.*, vol. 55, no. 9, pp. 5174–5184, Sep. 2017, doi: 10.1109/Tgrs.2017.2703084.

[11] P. F. Alcantarilla et al., "Fast explicit diffusion for accelerated features in nonlinear scale spaces," in *Proc. Brit. Mach. Vis. Conf.*, 2013, pp. 1–11, doi: 10.5244/C.27.13.

[12] D. G. Lowe, "Distinctive image features from scale-invariant keypoints," *Int. J. Comput. Vis.*, vol. 60, pp. 91–110, Nov. 2004, doi: 10.1023/B:Visi.0000029664.99615.94.

[13] A. F. Martin and C. B. Robert, "Random sample consensus: A paradigm for model fitting with applications to image analysis and automated cartography," *Commun. ACM*, vol. 24, pp. 381–395, 1981.

[14] J. Karvonen, M. Simila, and J. Lehtiranta, "SAR-based estimation of the baltic sea ice motion," in *Proc. IEEE Int. Geosci. Remote Sens. Symp.*, 2007, pp. 2605–2608, doi: 10.1109/Igarss.2007.4423378.

Chaoyue Li received the B.S. degree in geomatics engineering from WuHan University, Wuhan, China, in 2020. He is currently working toward the Graduation degree in resource and environment with the School of Geospatial Engineering and Science, Sun Yat-sen University, Guangdong, China.

His research focuses on remote sensing applications in Arctic sea ice drift.

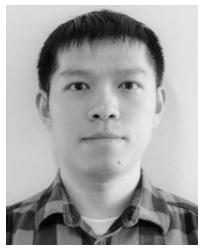

Gang Li received the M.Phil. degree in geodesy and engineering from the Institute of Seismology, China Earthquake Administration, Wuhan, China, in 2012, and the Ph.D. degree in earth system geoinformation science from the Chinese University of Hong Kong, Hong Kong, in 2017.

Since 2020, he has been with the School of Geospatial Engineering and Science, Sun Yat-sen University, Guangdong, China. His research interests include high-mountains Asia, Greenland, and Arctic Ocean, and SAR remote sensing application in different fields, especially for the cryosphere dynamic.

Zhuoqi Chen received the B.S. degree in geography from Beijing Normal University, Beijing, China, in 2003, and the Ph.D. degree in cartography and geographical information system from the Institute of Geographic Sciences and Natural Resources Research, Chinese Academy of Sciences, Beijing, China, in 2009.

He is currently an Associate Professor with the School of Geospatial Engineering and Science, Sun Yat-sen University, Guangdong, China. His research focuses on remote sensing applications in ecological model and hydrometeorology.

Xue Wang received the B.S. degree in geographical information science and the M.S. degree in photogrammetry and remote sensing from Peking University, Beijing, China, in 2012 and 2015, respectively, and the Ph.D. degree in geography and resource managemen from The Chinese University of Hong Kong, Hong Kong, in 2019.

She is currently an Assistant Professor with the School of Geospatial Engineering and Science, Sun Yat-sen University, Guangdong, China. She is also a Key Member of the Polar Oceans and Climate Change Innovation Team, Southern Marine Science and Engineering Guangdong Laboratory, Zhuhai, China. Her research interests include polar remote sensing and sea ice drift retrieval.

Xiao Cheng received the M.S. degree in geodesy and measurement engineering from the University of Wuhan, Wuhan, China, in 2001, and the Ph.D. degree in cartography and geographic information systems from the Chinese Academy of Sciences, Beijing, China, in 2004.

He is currently the Dean of the School of Geospatial Engineering and Science, Sun Yat-sen University, Guangdong, China, where he is also a Professor of polar remote sensing and climate change. He had gone to Antarctic three times in 1999, 2005, and 2007, and gone to Arctic two times in 2013 and 2014 for science expedition. His research interests include the observation of climate change impacts on polar regions, including ice sheets and ice shelf, sea ice, and land cover mapping using remote sensing methods related to these.